The effect of deep brain structure modeling on transcranial direct current stimulation-induced electric fields: An in-silico study

Chae-Bin Song, Cheolki Lim, Jongseung Lee, Donghyeon Kim*, Hyeon Seo*

***Abstract*— To study transcranial direct current stimulation (tDCS) and its effect on the brain, it could be useful to predict the distribution of the electric field induced in the brain with given tDCS parameters. As a solution, simulation with realistic computational models using magnetic resonance images (MRIs) have been widely used in the fields. With the recent advance of deep learning-based segmentation techniques of the brain, questions have been raised about if tDCS-induced electric field is affected by the deep brain structures. This study aimed to investigate the effect of the deep brain structure modeling on the induced electric field. To this end, we generated models with and without the deep brain structures by using an open MRI dataset comprising tDCS parameters, electric field simulation results and in-vivo intracranial recordings in the deep brain structures. We investigated the difference between the simulation results of the two models with a statistical analysis. Our results indicated that tDCS-induced electric fields and current flow in the brain are significantly different when the deep brain structures are considered.**

I. Introduction

tDCS is one of the non-invasive electrical brain stimulation modalities to modulate cortical activities by delivering weak direct currents to the scalp [1]. Various factors affecting tDCS-induced electric fields include external factors, tDCS doe parameters, and internal ones, the anatomical structures of an individual's brain. Even if the external factors set the same, distribution of the electric field could be differed by the internal factors. The direction and intensity of tDCS-induced electric field showed intra- and inter-subject variability because of individual differences of brain anatomy. Therefore, it is important to predict the distribution of the electric fields induced in the brain.

MRI-based computational models are widely accepted techniques to estimate the direct current-induced electric field distributions across the brain segmental regions [2]. The overall pipeline of tDCS simulation comprises a modeling pipeline and a computation pipeline. The modeling pipeline includes segmenting the MRI into different tissue compartments and generating 3D tetrahedral meshes from the segmented MRI. The computation pipeline comprises defining a tDCS simulation problem and solving it based on the finite element method (FEM) procedure [3]. SimNIBS [4] and ROAST [5] are the most widely used software with an end-to-end pipeline for transcranial electrical stimulation (tES) simulation research. They create models from segmented MRIs with five tissue layers (gray matter (GM), white matter (WM), cerebrospinal fluid (CSF), skull, and scalp).

Recently, many research groups have developed the segmentation of deep brain structures [6], [7]. According to these previous studies, precise segmentation of the deep brain structures affects tDCS-generated electric fields. The previous studies expected that it would have a great impact on the clinical outcomes. Especially certain deep brain structure is associated with specific disease, such as amygdala being related with Alzheimer's disease [8]. Thus modeling each deep brain structrue might be important when conducting tDCS simulation for patients with such diseases. In other side, there are issues regarding the effect of tDCS on deep brain structures. It remains controversial that tDCS could modulate brain activity in the deep brain structures [9], [10].

Here, we aim to investigate the effects of the deep brain structures on the tDCS-induced electric field. To consider the deep brain structure, we used an end-to-end solution for tES simulation, namely tES LAB (Neurophet Inc., Seoul, Korea). It is because this tool provides deep learning-based fine segmentation of the deep brain structures and computation of the electric field. Therefore, we generated two anatomical head models with and without the deep brain structures. With this goal, we used an experimental dataset [2] that offers in vivo intracranial recordings near the hippocampus with its corresponding simulation results, and the simulation results with and without deep brain structures were compared with the intracranial recording dataset.

II. Methods

A. The pipeline of tES LAB

To construct computational models for tDCS, we used tES LAB for modeling and simulation. Fig. 1 shows two candidates for the pipelines of tES LAB. A segmentation process is a deep learning-based brain segmentation model, called Split-Attention U-Net (SAU-Net) [11] based on an encoder-decoder. In pipeline a, SAU-Net segments the brain MRI into cerebral GM, cerebral WM, cerebellar GM, cerebellar WM, ventricles, CSF, skull, and skin (8 tissue labels, Default mode). In pipeline b, SAU-Net conducts more fine segmentation for deep brain structures (thalamus, caudate, putamen, pallidum, hippocampus, amygdala, and accumbens) [7] and eyes (16 tissue labels, Fine mode).

C.-B. Song, J. Lee, and D. Kim is with the Research Institute, Neurophet, Inc., Seoul, 06234, South Korea (e-mail: cbsong@neurophet.com, jonseunlee@neurophet.com, corresponding author to provide phone: +82-2-6954-7971; fax: +82-2-6954-7972; e-mail: donghyeon.kim@neurophet.com).

C. Lim is with the School of Electrical Engineering and Computer Science, Gwangju Institute of Science and Technology, Gwangju, 61005, South Korea (e-mail: chim@gist.ac.kr).

H. Seo is with the Department of Computer Science, Gyeongsang National University, Gyeongsangnam-do, 52828, South Korea (corresponding author to provide phone: +82-55-772-1385; e-mail: hseo0612@gnu.ac.kr).

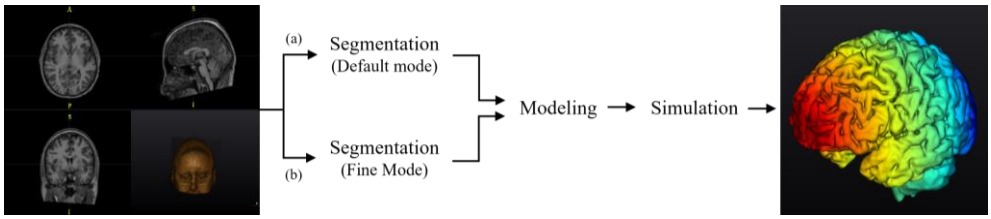

Fig. 1. Flowchart of tES LAB. (a) and (b) are the candidate pipelines that operate based on models with eight and sixteen tissue layers, respectively.

The mesh generation algorithm and the Laplacian equation solving algorithm are commonly used in all pipelines. A default model is a model created based on segmented MRI in pipeline (Fig. 1 a) and has eight tissue layers. A fine model is created based on the output of SAU-Net in pipeline b (Fig. 1b) and has sixteen tissue layers. After the modeling pipeline, we placed the stimulation electrodes at the same positions as in the previous study [2], which provide in vivo intracranial recordings under tES. In the computation pipeline, the FEM algorithm transformed the Maxwell equation into a weak formulation and set the FEM problem with the Galerkin method. The Eigen library was used as a solver along with FEM algorithms to compute the electric field.

Huang et al. estimated the optimal conductivities for each subject to accurately reflect the field [2]. These optimal values differ considerably across subjects as they account for soft tissues such as muscle and fat. We assigned the median of the optimal conductivities proposed by Huang et al. In Huang's study, they did not incorporate anatomical information of the deep brain structures for model-predicted voltage. As far as we know, research on the conductivity of all the deep brain structures has not yet been activated because it is difficult to study the conductivity of the deep brain structures. Thus, we assigned electrical conductivities according to the previous studies for the conductivity of each structure [6], [12]–[14]. According to studies on conductivities [15], [16], it is important to precisely assign the conductivity of each tissue to reduce errors in calculating the electric field. The conductivities we assigned to brain regions are listed in TABLE I.

TABLE I. Conductivities of each brain region

Region	***Cond*** †	***Ref.***	***Region***	***Cond***	***Ref.***
Cererbral GM	0.82	[2]	Eyes	0.500	[16]
Cerebral WM	0.38	[2]	Thalamus	0.475	[11]
Cerebellar GM	0.82	[2]	Caudate	0.632	[12]
Cerebellar WM	0.38	[2]	Putamen	0.561	[12]
Ventricles	1.65	[2]	Pallidum	0.120	[13]
CSF	1.65	[2]	Amygdala	0.120	[13]
Skull	0.03	[2]	Hippocampus	0.419	[11]
Skin	0.29	[2]	Accumbens	0.200	[6]

† Cond: Conductivity (S/m)

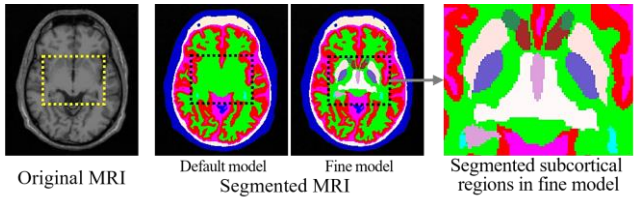

Fig. 2. Original, segmented MRIs for the default and the fine models, and the segmented deep brain structures (P06)

B. *Data & Analysis*

The dataset [2] provided T1-weighted MRIs, the segmentation data, and the voltage recording data for ten subjects. The segmentation data consisted of the five tissues (WM, GM, CSF, skull, and scalp) along with annotations of the extra-cranial stimulation electrodes, subgaleal electrodes, intracranial electrode strip, and the surgical drain. The voltage magnitude was derived from the in vivo recordings of the electrical potential induced by tES. To measure the voltage magnitude, the authors used cortical electrodes (grid arrays and linear strips) and depth electrodes. They placed cortical electrodes on the cortex and inserted depth electrodes around the hippocampus. They provided the locations of the electrodes in MNI and voxel coordinates. Prior to analysis of simulation results of tES LAB, we converted the coordinates for tES LAB to MNI, since the coordinates of the recording electrode locations were MNI. If the location or voltage value in the dataset is described as 'NaN', we deleted the information on that electrode. The 2 x 2 cm^2 were placed on Fpz-Oz.

We reported analysis results in two aspects: (1) comparing the voltages of the model with and without the mesh of the deep brain structures, and (2) analyzing the correlation. between the predicted values of tES LAB and the recorded value.

To investigate the voltage differences between the models with and without meshes of deep brain structures, we conducted a statistical analysis. The location and number of recording electrodes were different for all subjects. For example, one electrode was placed in the cerebral GM, while the other was placed in a deep brain region. The different tissue where the electrode was located indicated that the conductivity that affects the current flow was also different. Due to the difference, the distribution of voltage data for each subject did not follow the Gaussian distribution. Since it does not follow a Gaussian distribution, we used the Wilcoxon matched-pairs signed-rank test (alpha = 0.05) as non-parametric tests. The results of the statistical analysis represent significant differences in the mean of the paired observations.

To evaluate the correlation between the predicted voltage of tES LAB and the recorded voltage in vivo, we analyzed correlation. The correlation coefficient is a statistical measure of the strength of a linear relationship between two variables [17]. It might be interpreted as the degree to which one variable explains another variable. By analyzing the correlation, we tried to investigate linear relationships between the recorded and predicted values.

III. RESULTS

A. *Segmentation of the deep brain structures*

We created the default model with eight tissue labels and the fine model with labels for the deep brain structures and

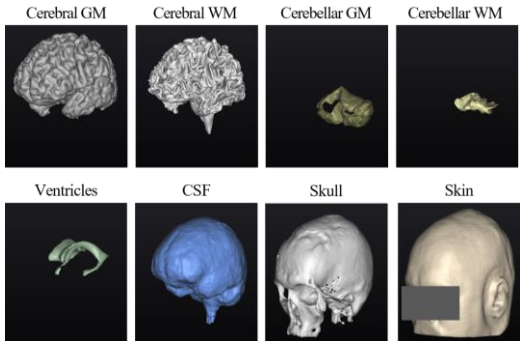

Fig. 3. The 3D tetrahedral mesh for eight common brain regions in the default and the fine model (P06)

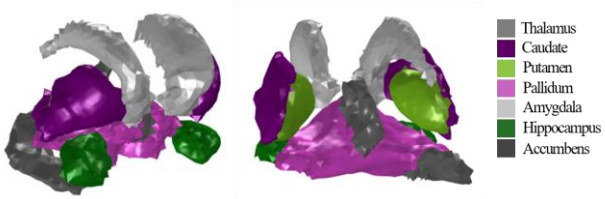

Fig. 4. The 3D tetrahedral mesh-based models of the deep brain structures (P06)

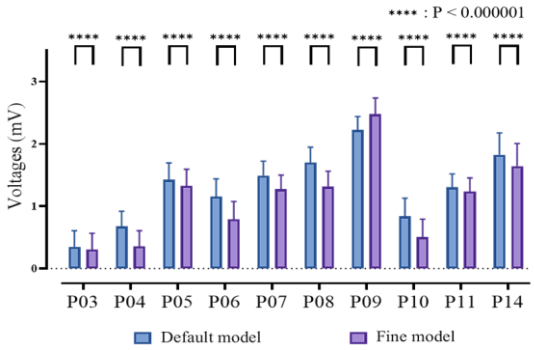

Fig. 5. Comparison of the voltages for the default and the fine models

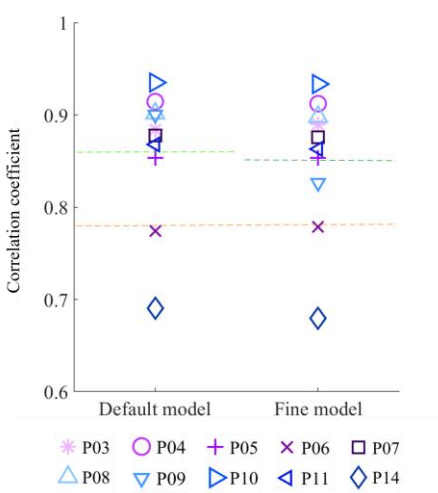

Fig. 6. Correlation coefficient for two models with intracranial recordings. Each subject is represented by a different symbol as indicated by the legend of the figure. Light and dark green dash lines are respectively represented the average values for the default and the fine models. Orange one is the average value in the previous study.

eyes. Fig. 2 shows the axial brain slices of the original and segmented MRI in the default and fine models for one subject (P06). The fine model has eight common tissue labels in the default model and additional labels for deep brain structures and eyes.

B. Models for the deep brain structures

Fig. 3 is about the eight tissue types that the default and fine models have in common for P06. The 3D meshes were generated for the seven the deep brain structures based on the segmentation results for the deep brain structures. The tetrahedral meshes of the deep brain structures for P06 are shown in Fig. 4.

C. Comparison of the default and fine models

We conducted the Wilcoxon matched-pairs signed-rank test to compare the voltage values in the default and the fine models. Fig. 5 shows the average voltage of the two models for all subjects. The error bars represent the standard error of the mean. There was a significant difference between the voltages of the two models. The voltage values had variations across all subjects due to variations caused by different geometrical features. Nine out of ten show higher voltage values of the default model than the fine model. However, the value of the fine model was large compared to the default model for P09.

D. Comparison with intracranial recordings

Fig. 6 shows the correlation coefficient for each subject and model in all electrodes. In the previous study [2], P10 and P14 showed the highest and lowest prediction results. Likewise, P10 showed the highest correlation coefficient in the simulation results. The prediction is poor for P14 as shown in the correlation coefficient.

The previous study analyzed the correlation based on individually optimized conductivities. Their models provide predictions of the magnitudes with an accuracy of 0.86 and 0.88, respectively, for the cortical and the depth electrodes across all subjects. In the simulation with tES LAB, we analyzed the correlation using the median value of the optimized conductivities. The average for all electrodes was 0.86 ± 0.07 for the default model and 0.85 ± 0.07 for the fine model. Our results showed a strong positive linear relationship between the recorded and predicted values for both the cortical and the depth electrodes [17].

IV. DISCUSSION

In our current work, we analyzed the effect of deep brain structures modeling on the tDCS simulation results. We used a dataset that provides intracranial recordings in cortical and deep brain structures. Separate segmentation pipelines were built for deep brain structures. We tried to create a model that reflects the properties of each structure. Especially, since each structure was modeled in the fine model, conductivities corresponding to each region were assigned. This allowed us to compare tDCS-induced electric fields.

Statistical analysis was conducted to investigate differences in voltage values between the default and fine models. Significant differences between the voltage values of the two models were shown for all subjects. We speculated

that the reason for the difference might be the additional layer of deep brain structures with different conductivities.

We focused on the difference between the default and the fine models. Nine out of ten subjects yielded higher voltages in the default model, but P09 showed the opposite result. We considered that the reason for the contradictory trend in P09 might be the different numbers and locations of the recording electrodes in all subjects. Therefore, we examined the number of cortical and depth electrodes. In most subjects, the average proportion of depth electrodes was 30%. Conversely, the ratio in P09 was 3%. We considered that a higher value in the fine model was observed due to the relatively small number of depth electrodes near the hippocampus for P09.

We speculated that additional layers of the deep brain structures with different conductivities might affect the voltages from the depth electrodes in the fine model. According to previous studies [18], since current flow is sensitive to tissue anatomy and conductivity, it is greatly influenced by mesh boundaries where conductivity changes. In the deeper region where the current flows across more boundaries, the current might decrease. Thus, we considered that the higher voltage in the fine model for P09 was a consequence of a relatively smaller measurement in the deep brain structures due to the small number of depth electrodes.

Additional analysis was conducted to examine how well the simulation results of tES LAB predict in vivo measurements. We investigated the correlation coefficients between the recorded and simulated values. The results for the correlation could be interpreted to indicate that the simulation results have a strong positive linear relationship with in vivo intracranial recordings [17].

When comparing the correlation coefficient between the default and fine models, the default model showed larger values than the fine model. We thought the cause might be conductivity. The common tissue layers in both models were assigned the conductivity used in the previous study [2]. On the other hand, we assigned the conductivities of the deep brain structures based on other previous studies [6], [12]–[14]. Since the conductivity of each subject was relatively less reflected for the deep brain structures, we speculated that the default model showed a higher correlation coefficient.

Future studies might need to analyze tDCS-induced electric fields and current flow based on fine models that consider anatomical features and conductivities. This study highlighted that the model with and without the deep brain structures showed differences in the tDCS simulation results. We want to refer that the results and all the differences presented in this study do not indicate a better or worse prediction of the electric field and the current flows induced in the brain by tDCS.

ACKNOWLEDGMENT

We would like to express our deep appreciation to the Research Institute of Neurophet Inc. for helping improve the performance of tES LAB by developing a deep learning-based segmentation model.

REFERENCES

[1] A. R. Brunoni, M. A. Nitsche, N. Bolognini, M. Bikson, T. Wagner, L. Merabet, D. J. Edwards, A. Valero-Cabre, A. Rotenberg, A. Pascual-Leone, R, Ferrucci, A. Priori, P. S. Boggio, and F. Fregni, "Clinical research with transcranial direct current stimulation (tDCS): Challenges and future directions," *Brain Stimulation*, vol. 5, no. 3. pp. 175–195, Jul. 2012.

[2] Y. Huang, A. A. Liu, B. Lafon, D. Friedman, M. Dayan, X. Wang, M. Bikson, W. K. Doyle, O. Devinsky, and L. C. Parra, "Measurements and models of electric fields in the in vivo human brain during transcranial electric stimulation," *eLife*, 2017.

[3] A. Datta, V. Bansal, J. Diaz, J. Patel, D. Reato, and M. Bikson, "Gyri-precise head model of transcranial direct current stimulation: Improved spatial focality using a ring electrode versus conventional rectangular pad," *Brain Stimulation*, vol. 2, no. 4, pp. 201-207.e1, Oct. 2009.

[4] A. Thielscher, A. Antunes, and G. B. Saturnino, "Field modeling for transcranial magnetic stimulation: A useful tool to understand the physiological effects of TMS?," in *2015 37th Annual International Conference of the IEEE Engineering in Medicine and Biology Society (EMBC)*, Aug. 2015, pp. 222–225.

[5] Y. Huang, A. Datta, M. Bikson, and L. C. Parra, "Realistic volumetric-approach to simulate transcranial electric stimulation - ROAST - a fully automated open-source pipeline," *Journal of Neural Engineering*, vol. 16, no. 5, Jul. 2019.

[6] E. A. Rashed, J. Gomez-Tames, and A. Hirata, "End-to-end semantic segmentation of personalized deep brain structures for non-invasive brain stimulation," *Neural Networks*, vol. 125, pp. 233-244, May. 2020.

[7] S. Louviot, L. Tyvaert, L. G. Maillard, S. Colnat-Coulbois, J. Dmochowski, and L. Koessler, "Transcranial Electrical Stimulation generates electric fields in deep human brain structures," *Brain Stimulation*, vol. 15, no. 1, pp. 1–12, Jan. 2022.

[8] S.P. Poulin, R. Dautoff, J. C. Morris, L. F. Barrett, B. C. Dickerson, and Alzheimer's Disease Neuroimaging Initiative, "Amygdala atrophy is prominent in early Alzheimer's disease and relates to symptom severity," *Psychiatry Research: Neuroimaging*, vol. 194, pp. 7-13, June 2011.

[9] D. Adair, D. Truong, Z. Esmaeilpour, N. Gedbodh, H. Borges, L Ho, J. D. Bremner, B. W. Badran, V. Napadow, V. P. Clark, and M. Bikson, "Electrical stimulation of cranial nerves in cognition and disease," *Brain Stimulation*, vol. 13, no. 3, pp. 717–750, May 2020.

[10] S. Vanneste, A. Mohan, H. B. Yoo, Y. Huang, A. M. Luckey, S. L. McLeod, M. N. Tabet, R. R. Souza, C. K. McIntyre, S. Chapman, I. H. Robertson, and W. T. To, "The peripheral effect of direct current stimulation on brain circuits involving memory," *Science Advances*, vol. 6, no. 45, Nov. 2020.

[11] M. Lee, J. Kim, R. E. Y. Kim, H. G. Kim, S. W. Oh, M. K. Lee, S.-M. Wang, N.-Y. Kim, D. W. Kang, Z. Rieu, J. H. Yong, D. Kim, and H. K. Lim, "Split-attention u-net: A fully convolutional network for robust multi-label segmentation from brain mri," *Brain Sciences*, vol. 10, no. 12, pp. 1–22, Dec. 2020.

[12] H. McCann, G. Pisano, and L. Beltrachini, "Variation in Reported Human Head Tissue Electrical Conductivity Values," *Brain Topography*, vol. 32, no. 5, pp. 825–858, Sep. 2019.

[13] M. Akhtari, M. Mandelkern, D. Bui, N. Salamon, H. v. Vinters, and G. W. Mathern, "Variable Anisotropic Brain Electrical Conductivities in Epileptogenic Foci," *Brain Topography*, vol. 23, no. 3, pp. 292–300, Sep. 2010.

[14] P. Hasgall, E. Neufeld, M. C. Gosselin, A. Klingenböck, N. Kuster, P. Hasgall, and M. Gosselin, "IT'IS Database for thermal and electromagnetic parameters of biological tissues," *IT'IS Database ver. 4.1*, Feb. 22, 2022.

[15] E. Michel, D. Hernandez, and S. Y. Lee, "Electrical conductivity and permittivity maps of brain tissues derived from water content based on T1-weighted acquisition," *Magnetic Resonance in Medicine*, vol. 77, no. 3, pp. 1094–1103, Mar. 2017.

[16] J. Gomez-Tames, A. Hamasaka, A. Hirata, I. Laakso, M. Lu, and S. Ueno, "Group-level analysis of induced electric field in deep brain regions by different TMS coils," *Physics in Medicine & Biology*, vol. 65, no. 2, Jan. 2020.

[17] A. Opitz, W. Paulus, S. Will, A. Antunes, and A. Thielscher, "Determinants of the electric field during transcranial direct current stimulation," *Neuroimage*, vol. 109, pp. 140–150, Apr. 2015.

[18] B. Ratner, "The correlation coefficient: Its values range between +1/−1, or do they?," *Journal of Targeting, Measurement and Analysis for Marketing*, vol. 17, no. 2, pp. 139–142, Jun. 2009.

[19] M. Bikson, A. Rahman, and A. Datta, "Computational models of transcranial direct current stimulation," *Clinical EEG and Neuroscience*, vol. 43, no. 3, pp. 176–183, Jul. 2012.